# Analysis of a spatial structure of a focused x-ray beam diffracted from crystals

A. Kazimirov*[a], V. Kohn[b], A. Snigirev[c], and I. Snigireva[c]
[a]Cornell High Energy Synchrotron Source (CHESS), Cornell University, Ithaca, New-York, 14853;
[b]Russian Research Center "Kurchatov Institute", 123182 Moscow, Russia;
[c]European Synchrotron Radiation Facility (ESRF) 6 rue Jules Horowitz 38043 Grenoble, France

*ayk7@cornell.edu; phone (607)255-2538; fax (607)255-9001;

## ABSTRACT

Spatial structure of a focused beam diffracted from crystals of different thickness was studied experimentally at the ESRF optical beamline BM5. The beam was focused by a planar parabolic refractive lens. Si (111) thick crystal and 8 μm and 50 μm thick perfect Si(111) crystals positioned between the lens and the focus were used as model samples. The structure of the beam was analyzed at the focus of the lens by using a knife edge scan and a high-resolution CCD camera. The broadening of the focused beam due to the extinction effect was experimentally measured and compared with theoretical predictions. For a sufficiently thin crystal a second peak was experimentally observed which is due to the reflection from the back surface. We found also that the spatial structure depends on whether the crystal diffracts strongly (dynamically) or weakly (kinematically). In the later case, both surfaces of the crystal effectively reflect as mirrors with the reduced reflectivity and the relative intensity of the two peaks is determined by absorption. Theoretical simulations show excellent agreement with experiment.

**Keywords:** X-ray optics, Bragg diffraction, crystals, X-ray focusing, refractive lenses

## 1. INTRODUCTION

Diffraction of a focused X-ray beam can be viewed as a part of a more general problem of diffraction of an arbitrary incident wave by crystals. Theoretical development of this general problem was the subject of the extensive theoretical work in 1960s and 70s (see textbooks [1] and references there). The problem in the Bragg case of diffraction has been successfully solved independently by Afanas'ev and Kohn [2] and Uragami [3]. In particular, in [2] an analytical solution for the Bragg diffraction of an X-ray wave formed by an infinitely narrow slit in front of the crystal surface was derived and interesting physical effects have been predicted and analyzed theoretically. One of them is the broadening of the initially infinitely narrow beam by crystal which is a consequence of the extinction effect. For a sufficiently thin crystal the second peak appears which corresponds to the scattering from the back surface of the crystal (Fig.4 in [2]). These effects have not been observed for a long time because of the obvious experimental difficulties of placing both a narrow slit and a detector (film) very close to the crystal surface. The same problem was also the main obstacle on the way of the development of X-ray section topography (in a strict sense) in the Bragg geometry: instead, the Berg-Barrett technique with a narrow slit of typically few tens of microns was developed and utilized.

Recently, the diffraction of a focused beam was studied theoretically [4,5]. It was shown that for the focused beam the diffraction physics is fully analogous to the case of an infinitely narrow slit on a crystal surface and the structure of the beam in the focus shows all the features predicted theoretically. Moreover, using the focused beam solves the main experimental problem mentioned above as the crystal can now be placed anywhere between the focusing optics and the focus. New diffraction imaging technique has been proposed [5] based on the prediction that any interface or a defect will break up the destructive interference inside the crystal and can be visualized, thus presenting a realistic approach for a "truly" section topography in the Bragg case.

First experiments have been performed in [6,7] by using a phase zone plate (ZP) as a focusing optics producing 200 nm beam. These experiments fully confirmed the theoretical predictions: the broadening of the focused beam by the extinction effect was observed for the first time; the peaks from the back surface of 4.5 to 25 μm thick Si layers were

Advances in X-Ray/EUV Optics and Components IV, edited by Ali M. Khounsary, Christian Morawe, Shunji Goto,
Proc. of SPIE Vol. 7448, 74480P · © 2009 SPIE · CCC code: 0277-786X/09/$18 · doi: 10.1117/12.826082

also observed; and the structural sensitivity was demonstrated as the SOI layers used in these experiments were not perfect. Still, the detailed comparison with theoretical calculations required perfect crystals. Also, calculation of the diffraction patterns produced by the ZP involves modeling propagation of the wave through several additional paths due to the presence of such additional elements as the beam stop and the order sorting aperture before the wave reaches the crystal. Though these computational difficulties were successfully solved in [6,7], they present additional complication. On the other hand, for the refractive lens the propagator through the refractive lenses can be expressed analytically and in a thin lens approximation which is sufficient in most cases is approximated by a simple exponential function [8] thus significantly simplifying the theoretical analysis. The purpose of this work was to use planar parabolic refractive lenses and perfect Si crystals of different thickness to perform the detailed comparison with theory.

The article is organized as follows. In the next section, the experimental setup is presented and discussed. In Section 3, the experimental results from the thick perfect Si crystal and thin perfect Si crystals of the thickness of 8 and 50 μm are presented. In Section 4, we will discuss these results followed by conclusions and the outlook for a future work.

## 2. EXPERIMENTAL SETUP

The experiment was performed at the bending magnet ESRF optical beamline BM5. Experimental results presented and discussed below were obtained at the energy of 23.0 keV selected by an upstream double-crystal Si(111) monochromator. Planar compound refractive lenses (CRL) was used to focus the X-ray beam [9]. The CRL composed of different numbers of individual lenses on a single chip were produced on a Si wafer by using a modern microfabrication technology which involves photolithography and reactive ion etching. The lenses depth was 50 μm with the web thickness of 2 μm (see [9] for details). For this particular energy the array consisting of 28 individual lenses was used with the total thickness of 1.45 mm. The distance from the source to the lens $L_S$ was 55 m. The effective lens aperture $A_\gamma$ was calculated as 47 μm which was comparable to the size of the real aperture. The focal length $F=R/(2N\delta)$, where $R$ is the radius of the individual lens, $N = 28$, and $\delta$ is the decrement of the refractive index, was calculated as 24.42 cm and the focus distance as $L_f = F/(1 - F/L_S) = 24.56$ cm with the experimentally measured focus distance of 24.2 cm.

The experimental setup (Fig.1) was assembled on a micro-optics test bench equipped with precise stages for accurate alignment of all optical components [10]. The CRL chip was mounted on an optical stage with 5 degrees of freedom (two translational and three rotational) for the alignment of the lens in the beam. Crystals were mounted on a diagnostic/sample stage with the added Huber rotational segment allowing for a crystal rotation within the 20 deg. angular range. On a detector stage, either a knife edge (200 μm diameter Pt wire), or a high-resolution CCD detector was mounted. SensicamQE 12 bit camera with 1376 × 1040 pixels and 6.45 μm × 6.45 μm pixel size with the Olympus UPLAPO x10, NA = 0.4, objective was used for a high-resolution imaging. As a scintillator, the 9.9 μm thick LAG: Eu film on 170 μm YAG substrate was used providing a spatial resolution better than 1.3 μm (estimated value).

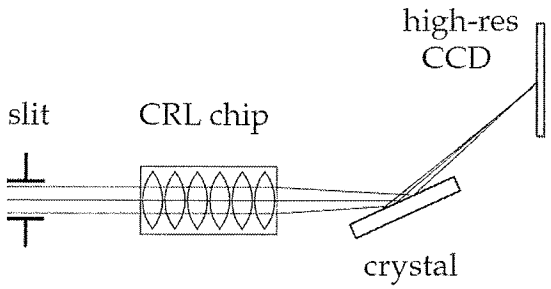


Fig. 1. The experiment setup at the ESRF optical beamline BM5. The incident beam of the energy of 23.0 keV was selected by a Huber slit and focused by the CRL lens. The crystals were mounted on a rotation stage positioned between the CRL chip and the lens focus. The spatial distribution of the diffracted intensity was measured at the lens focus by a high-resolution CCD camera or a knife edge (not shown).

The detector was positioned exactly at the focus, and the crystal between the lens and the focus. The long focal distance provided by refractive lenses allowed for plenty of space for a comfortable mounting of crystals of the size of a few cm

(for comparison, in our ZP setup at the APS 2-ID-D beamline [6,7] crystals were mounted on a sample holder of a 6-circle diffractometer within the 13 mm distance between the order sorting aperture and the zone plate focus). The Huber slit mounted on a separate movable stage defined the size of the beam incident on the CRL, typically of 40 μm vertically by 30 to 100 μm horizontally.

As an example, the experimental high-resolution image of the beam diffracted from the 50 μm thick Si crystal, (111) reflection, and recorded in the lens focus is shown in Fig. 2. This image is formed by two parts of the beam. The left part is produced by the beam intercepted and focused by the CRL chip. The right part is produced by the incident beam that was not intercepted by the lens and was unfocused; its vertical size was defined by the Huber slit. The cross sections through the part of the image produced by the focused beam, section A, and by the unfocused beam, section B, are shown on the right panel of the Fig.2. This particular crystal was thick enough to observe the beam reflected from the back surface even for the beam of 30 μm wide defined by the slit, similar to the experiment reported in [11] by using 50 μm wide slit. Therefore, both sections show two beams, the one reflected from the front surface of the crystal, and the second one reflected from the back surface with the distance between them defined by the crystal thickness and the Bragg angle. Obviously, the focused beam reflected from the front surface shown in the section A is very narrow. Still, as we will see in the next section, the measurements performed by the knife edge technique revealed the broadening of the focused beam relative to the beam without the crystal due to the extinction effect, and this is one of the main results of our work. For comparison, the peak reflected from the back surface is shown also on a scale multiplied by a factor of 10. The detailed comparison of the experimental profiles with theory is performed in the next sections.

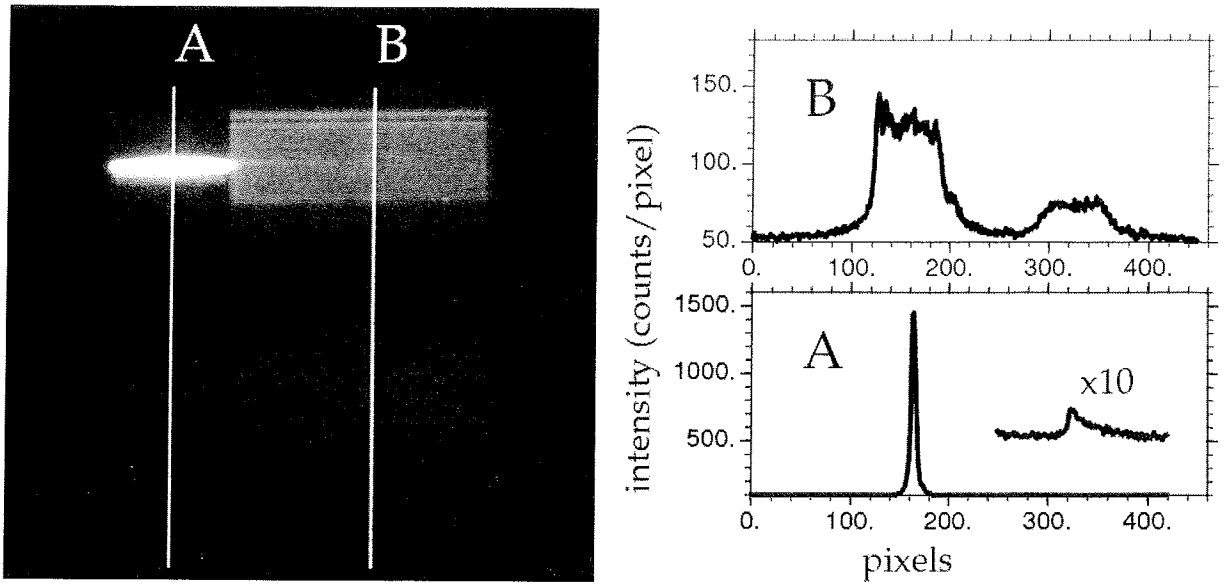


Fig. 2. Left panel: the experimental high-resolution CCD image of the beam diffracted from a 50 μm thick Si crystal recorded at the focus of the CRL lens. The left part of the image is produced by the beam focused by the CRL. The right part of the image is produced by the unfocused beam propagating parallel to the CRL chip surface and also diffracted from the same crystal. Right panel: cross sections through the left part of the image (focused beam, lower graph A) and the right part of the image (unfocused beam, upper plot B).

## 3. EXPERIMENTAL RESULTS

### 3.1 The size of the focused beam and the effective source size

The result of the knife edge scan through the focused beam at the focus of the lens is shown in the upper panel of Fig.3 by black circles. The derivative of this curve (open circles) gives the shape of the beam with the size (FWHM) of 0.92 μm. This size was much bigger than expected based on the characteristics of the lens tested earlier at other

beamlines. It was found that in this particular case the focusing was limited by the effective source size. Thin solid line is the theoretical curve calculated for the particular lens and experimental geometry using the source size as the only fitting parameter. The fit reveals the source size of 200 μm which was confirmed by the independent source size measurements by using the boron fiber interference technique [12]. The source size specified by the machine parameters is 80 μm [13]. It was determined that the reason for the significant broadening of the source size is the mechanical vibrations in the monochromator. Note here that mechanical vibrations and instabilities present the major problem for the third generation facilities in reaching their target performance parameters.

### 3.2 Thick crystal

To study the shape of the focused beam diffracted from the perfect thick crystal we used float zone Si(111) bulk crystal of 0.5 mm thickness and the knife edge technique. The lower panel in Fig.3 shows the experimental curve (solid circles) and its derivative (open circles). The broadening of the beam is clearly observed. Solid line is the theoretical curve calculated by using theoretical approach developed in [4,5]. The characteristics of the particular lens, our experimental geometry and experimentally determined effective source size were fixed and the only fitting parameter was the vertical scaling factor. As one can see, the agreement between the experiment and the theory is excellent.

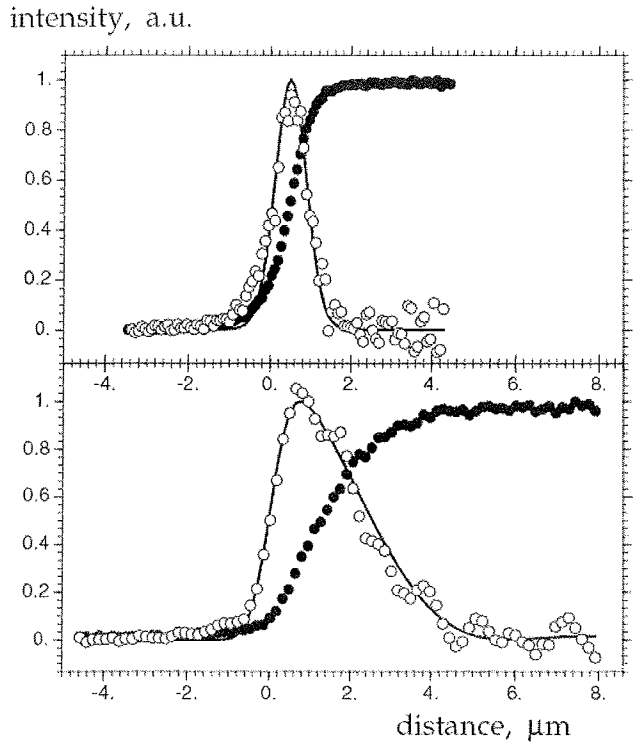


Fig. 3. Upper panel: knife edge scan through the focused beam (solid circles) and its derivative (open circles). The FWHM size in the focus is 0.92 μm. Thin solid line – theoretical curve calculated for fixed lens parameters and the experimental geometry, and the source size of 200 μm used as the only fitting parameter. Lower panel: knife edge scan through the focused beam (solid circles) diffracted from thick Si(111) crystal, 111 reflection and its derivative (open circles). The broadening relative to the beam without the crystal is clearly observed. Thin solid line – theoretical calculation performed without any fitting parameters (except for vertical scaling).

Note the following important features of this profile. The left side (the front rise) of the intensity curve is very sharp and it follows the shape of the incident focused beam (upper panel). The right side is a gradual decay of the intensity which reflects the penetration of the wave field in crystal. The shape of the beam will be discussed more in detail in Section 4.

### 3.3 Thin crystals

In our next experiment we studied the spatial structure of the beam diffracted from thin crystals: thin, 8 and 50 μm thick Si (111) oriented membranes produced by the chemical etching. For this experiment the high-resolution CCD camera was used as a detector. The CCD images (see Fig. 2) were taken at each angular point while scanning the sample through the (111) Bragg reflection. The cross sections of type A in Fig.2 for each angular position were composed in a 3D data set shown in Fig.4a. Here, two argument axes represent the spatial coordinate in units of the CCD pixels and the second axis is the angle. To obtain diffraction rocking curves the integration over the CCD pixels was performed for each angular position. Integration over pixels of the left and the right parts of the image corresponding to the focused and unfocused beams (see Fig.2 and explanations there) gives the diffraction curve from the sample measured with the focused beam through the lens angular aperture and with the collimated beam from the monochromator, correspondingly. These curves (background subtracted) are shown in Fig.4b and Fig.5b. The curve measured with the unfocused beam (solid line) is very narrow with the FWHM of less than 20 μrad with the calculated width for this energy

of 11.5 μrad indicating a high crystal quality. The curve measured with the focused beam is much broader with the FWHM of about 120 μrad which corresponds to the angular aperture of the lens.

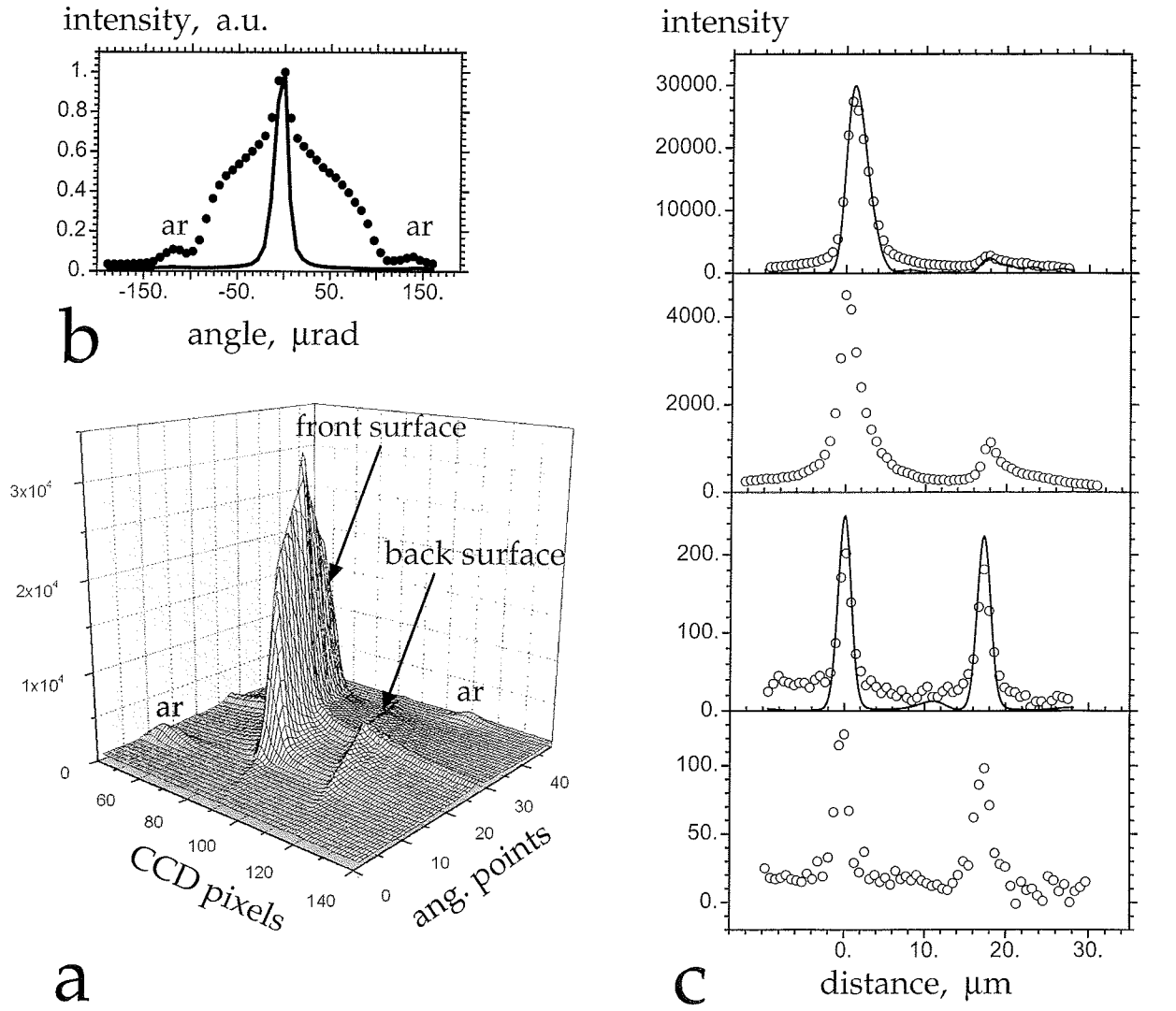


Fig.4. Experimental results for the perfect thin S(111) membrane of the thickness of 8 μm. (a) Sections through the diffraction images recorded by the high-resolution CCD camera at the focus of the lens (section A in Fig.2) composed for the angular points as the crystal was scanned through the Bragg (111) reflection. (b) Diffraction curves measured with the focused beam (solid circles) and unfocused beam (solid line). (c) Sections through the diffraction pattern recorded for different angular position from the center of the curve, from top to bottom: 35 μrad, 77 μrad, 140 μrad, and 175 μrad.

There are some artifacts related to our experimental setup. One of them is an additional intensity peak superimposed on the broad diffraction curve measured in the focused beam with its angular position lined up exactly with the maximum intensity for the unfocused beam. We attribute this rise in intensity to the contribution from the 3rd harmonic from the monochromator (333) reflection due to the fact that our setup does not have mirror. High energy harmonic penetrating silicon lenses almost without focusing will diffract from the sample at the same angle as the main harmonic for the (111) reflection. The high energy 3rd harmonic may explain also two small peaks on the sides of the diffraction curve in the focused beam marked by 'ar' on the plot. We found that they correspond to the small intensity regions in Fig.4a, also marked by 'ar'. We believe that they are produced by the small portions of the beam refracted by the tips of the slit blades. We verified this assumption by changing the position of the slit relative to the lens: the positions of the 'ar' peaks

also changes with distance and they were adjusted to minimize their interference with the main region of interest. The fact that these artifacts are clearly observed on diffraction curves confirms that perfect crystal can be used as an efficient analyzer revealing hidden details and setup misalignments, consistent with what we previously found working with the ZPs [6,7].

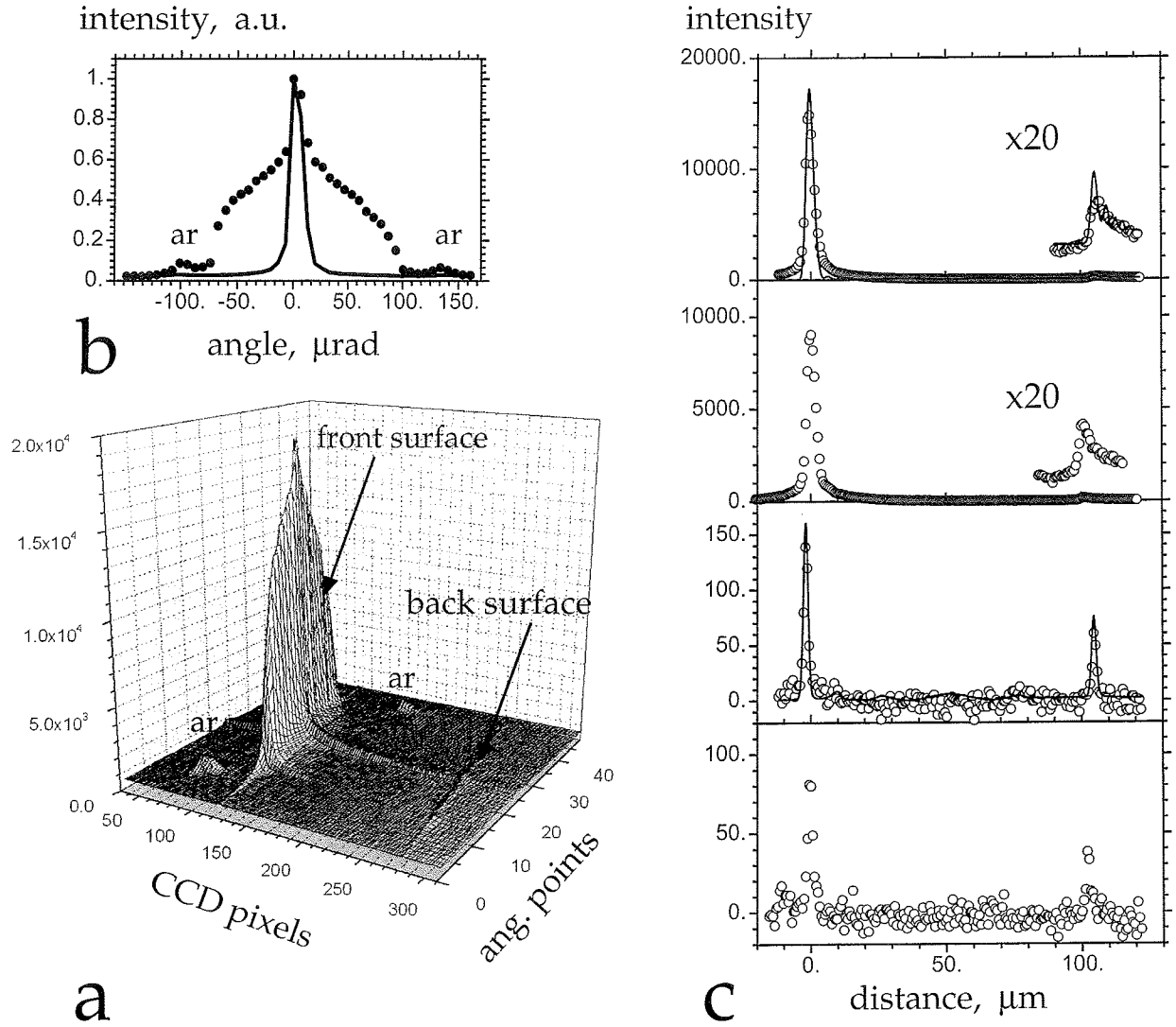


Fig. 5. The same as Fig.4, for perfect thin S(111) membrane of the thickness of 50 μm. (a) Sections through the diffraction images recorded by the high-resolution CCD camera at the focus of the lens (section A in Fig.2) composed for the angular points as the crystal was scanned through the Bragg (111) reflection. (b) Diffraction curve measured with the focused beam (solid circles) and unfocused beam (solid line). (c) Sections through the diffraction pattern recorded for different angular position from the center of the curve, from top to bottom: 35 μrad, 77 μrad, 140 μrad, and 175 μrad.

Selected cross sections through the diffraction pattern are shown in Fig.4c for different angular positions relative to the center of the lens angular aperture. On all plots two peaks are present, the first one positioned at zero is from the front surface and the second peak which corresponds to the reflection from the back surface. The position of the second peak is determined by the thickness of the crystal as $x = 2t\cos(\theta_B)$ [5]. The remarkable feature in Fig.4c is the change in the spatial structure with angle as the crystal is scanned away from the exact Bragg position. At the angle of 35 μrad from the center of the lens aperture (top plot) the first peak is about 10 times more intense than the peak from the back surface.

This plot corresponds to the angle at which the angular region of the total reflection is within the lens aperture. As the crystal is scanned away from the center the ratio of the two peaks changes and at the angle of 140 μrad (third plot from the top) their intensity becomes almost equal. At this angle the region of the total reflection is outside of the lens angular aperture. The observed transformation of the diffraction structure is due to the transition from the strong (dynamical) scattering to the weak (kinematical) scattering. Another feature is the change in the peaks width: as the total reflection region moves away from the aperture the peaks are getting sharper. This behavior is also consistent with the transformation from the dynamical to kinematical diffraction. The strong (dynamical) scattering takes place within the extinction distance from the surface. As the scattering becomes kinematical the scattering depth becomes narrower and this depth is inverse proportional to the angular deviations from the Bragg angle.

Solid lines in the profiles for 35 and 140 μrad are the theoretical curves calculated by using computational approach developed in [4,5]. The calculations were performed for perfect crystal, for given parameters of the lens, experimental geometry, and the experimentally determined effective source size. The only fitting parameters besides the scaling factor were the thickness of the crystal and the spatial resolution of the detector. The fit yielded the crystal thickness of 8.67 μm and the camera resolution of 1 μm.

The results for the 50 μm thick Si(111) crystal are shown in Fig.5. All features observed on the previous sample can be seen here, too. In the central angular region the peak from the back surface is now about 50 times weaker. Again, remarkable changes happen as we turn the crystal out of the lens angular aperture. At the angle of 140 μrad the second peak is only two times weaker than the peak from the front surface. The solid lines at the angles of 35 and 140 μrad are the theoretical fit with the same fitting parameters as for the thinner sample. The fit yielded the thickness of 50.54 μm and the camera resolution of 1 μm.

Since crystals have very narrow angular acceptance window, they select only small part of intensity from the focused beam making experiments described here intensity limited. Thus, typical exposure time to collect acceptable quality CCD images varied between 100 and 300 sec. The knife edge scans through the beam diffracted from thin crystals and epitaxial films were practically impossible. Undulator beamlines with about three orders of magnitude higher flux density and a much smaller effective source size are required for future experiments.

## DISCUSSION

The shape of the focused beam diffracted from thick perfect crystal (Fig.3) has two interesting features. First, the left side of the peak is sharp. For the lens of infinite aperture the sharpness is also infinite. It was first shown theoretically for the point source placed at the surface of the crystal [2,3]. For any real focused beam the rise of the intensity follows the shape of the focused beam [5]. This can be clearly seen from our results shown in Fig.3.

The second effect is the extinction effect, one of the most fundamental phenomena in X-ray diffraction. We remind here that at the center of the angular region of the total reflection the plane wave is attenuated in $e$ times at the depth from the surface of $L_{ex} = 2\sin(\theta_B)/(K|\chi_h|)$, where $\theta_B$ is the Bragg angle, $K = 2\pi/\lambda$, $\chi_h$ is the Fourier component of the crystal susceptibility. This depth $L_{ex}$ is called the extinction length. The X-ray intensity reflected from this depth will be shifted by the distance $x_{ex} = 2L_{ex}\cos(\theta_B)$ from the surface. In our case, $x_{ex} = 3.06$ μm, exactly as observed in the experiment. Extinction effect manifests itself in diffraction experiments in different ways [1]. Here, we have a unique opportunity to visualize this effect, i.e. to record X-ray intensity scattered from different depth from perfect crystal. In our recent experiments at the APS undulator beamline 2-ID-D we successfully visualized extinction effect for higher order and quasi-forbidden reflections [14].

Another interesting effect is the transformation of the diffraction pattern as the crystal moves away from the center of the lens angular aperture. This effect has not been observed experimentally or predicted theoretically before. As we already discussed in the experimental section two phenomena can be observed. First, the relative intensities of the peaks from the front surface and the back surface, dramatically different when the crystal is within the lens aperture, are becoming comparable when the crystal moves outside of the lens aperture. When the intensity of the diffracted beam is weak (kinematical diffraction) the relative intensity of these peaks is determined entirely by the absorption on the way of the beam from the front surface to the back surface and then back to the detector.

The second phenomenon accompanying kinematical diffraction manifests in two ways: both peaks are becoming sharper and their widths becoming equal. The later is not surprising as the broadening of the beam, as we just discussed, is due to the extinction effect and this is the feature of the strong dynamical scattering and the extinction vanishes on the tails of

the diffraction curve. To understand the effect of the peaks narrowing in a more formal way let us look at the analytical expression for the amplitude of the plane wave diffracted from the crystal of thickness $t$. For $q_0 >> Q$, where $Q = K\sqrt{2}(A_\gamma / F)$ is defined by the lens aperture $A_\gamma$, $K = 2\pi/\lambda$, $q_0$ is due to the angular shift of the crystal from the center of the lens angular aperture in the momentum space, we have

$$P_C(q - q_0) = -\frac{K\chi_h}{2q_0 \sin(2\theta_B)}\left[1 - \exp(-i(q - q_0)2d\cos\theta_B - \mu_0 t/\cos\theta_B)\right],$$

where $\mu_0$ is the absorption coefficient. This equation was derived from a more general expression for the propagator of the perfect crystal derived in [15] which is valid over all angular range including the region of the total reflection. Note also, that this equation describes the reflection of the plane wave from a thin crystal which is a subject of discussions in several textbooks on dynamical theory (e.g., section 4.9.3 in the book by Authier [1], see discussion and equations there). The subtraction of two exponential functions leads to the well known intensity oscillations in the angular space observed myriad times on the diffraction curves recorded from thin crystals and crystalline thin films by using sufficiently well collimated X-ray beam. To obtain the intensity distribution in the real space at the focus of the lens we have to apply the Fourier transformation to this equation. It can be easily shown that the Fourier transformation generates two delta-functions with the distance of $2d\cos(\theta_B)$ between them. These two peaks were experimentally observed in [6,7] and in this work. In a real experiment, the width of these two peaks is determined by the angular aperture of the lens and the source image. In our particular experiment the size of the focused beam was limited by the effective source size. When using 2D detector instead of a sharp knife edge, additional convolution with the detector point spread function is required. The sharpness of the peaks outside of the lens aperture makes this setup extremely sensitive instrument for precise measurements of the thickness of thin crystals and films.

As we just demonstrated, the peaks from the front and the back surfaces at the angles corresponding to the tails of the diffraction curve for extremely small beam is becoming more and more narrow with angle ideally approaching the delta-function (for a moment, we forget about the detector resolution). This phenomenon reflects the physical effect which is known and used for structural analysis: the depth of the surface layer from which X-rays scatter decreases with the angular deviation from the Bragg angle as $\propto 1/q$. Therefore, rocking curves become sensitive to a thinner and thinner layer as the crystal rotates away from the Bragg angle. In other words, information about thin layers contains on the tails of the rocking curves. This effect was established independently by Afanasev, *et al.* [16] and Robinson [17] and was called asymptotic diffraction or crystal truncation rod, correspondingly. By using technique described here we have a unique opportunity to visualize very thin layers provided that the focused beam is very small and the detector resolution is sufficiently high.

As we can see, analysis of the fine structure of the focused beam using the experimental approach discussed in this work is a new and exciting area of research which is based on the achievements of modern focusing optics and holds many interesting effects related to the fundamental phenomena of X-ray scattering as well as interesting potential applications.

## ACKNOWLEDGEMENTS

This work is based upon research conducted at the Cornell High Energy Synchrotron Source (CHESS) which is supported by the National Science Foundation and the National Institutes of Health/National Institute of General Medical Sciences under NSF award DMR-0225180. The work of V. Kohn is supported by RFBR grants 07-02-00067a and 09-02-12297-ofi_m. We acknowledge the European Synchrotron Radiation Facility for provision of synchrotron radiation facilities and we would like to thank the ESRF staff for assistance in using beamline BM5.

## REFERENCES

[1] Authier, A, [Dynamical theory of X-ray diffraction], Oxford University Press, Oxford, 2001; Pinsker, Z. G., [Dynamical scattering of x-rays in crystals], Berlin ; New York : Springer-Verlag, 1978.

[2] Afanas'ev, A. M. and Kohn, V. G., "Dynamical theory of X-Ray diffraction in crystals with defects", Acta Cryst. A. 27, 421 (1971).

[3] Uragami, T. S., "Pendellösung fringes in Bragg case in a crystal of finite thickness", J. Phys. Soc. Japan. 28, 1508 (1970).

[4] Kohn, V. G., "Diffraction reflection of a focused X-ray wave by a multilayer crystal ", Crystallogr. Rep. 51, 564 (2006).

[5] Kohn, V. G. and Kazimirov, A., "Simulations of Bragg diffraction of a focused x-ray beam by a single crystal with an epitaxial layer", Phys. Rev. B. 75, 224119 (2007).

[6] Kazimirov, A., Kohn, V. G., Cai, Z.-H., "Bragg diffraction of a focused x-ray beam as a new depth sensitive diagnostic tool", Proceedings of SPIE 7077, 70770L1 (2008).

[7] Kazimirov, A., Kohn, V. G., Cai, Z.-H., "New imaging technique based on diffraction of a focused x-ray beam", J.Phys.D.:Appl. Phys., Fast Track Communications 42, 012005 (2009).

[8] Kohn, V.G., "An exact theory of imaging with a parabolic continuously refractive X-ray lens", J. Exp. Theoret. Phys. (JETP) 97, 204 (2003).

[9] Snigirev, A., Snigireva, I., Grigoriev, M., Yunkin, V., Di Michiel, M., Kuznetsov, S. & Vaughan, G., "Silicon planar lenses for high energy X-ray nanofocusing ",Proc. of SPIE 6705, 670506 (2007).

[10] Snigirev, A., Hustache, R., Duboc, P., Massonnat, J.-Y., Claustre, L., Van Vaerenbergh, P., Snigireva, I., Grigoriev, M. & Yunkin, V., "Micro-optics test bench at the ESRF", Proc. of SPIE 6705, 670511 (2007).

[11] Yan, H. & Noyan, I.C., "Dynamical diffraction artifacts in Laue microdiffraction images", J.Appl.Phys. 98, 073527 (2005).

[12] Kohn, V., Snigireva, I. & Snigirev, A., "Direct measurement of transverse coherence length of hard X-rays from interference fringes", Phys. Rev. Lett. 85, 2745 (2000).

[13] http://www.esrf.eu/UsersAndScience/Experiments/Imaging/BM05/BM05characteristics.pdf

[14] Kazimirov, A., Kohn, V., Cai, Z.-H., in preparation.

[15] Kohn, V. G., Shvydko, Yu. V. and Gerdau, E.,"On the theory of an X-ray Fabry-Perot interferometer", Phys. Status Solidi B 221, 597 (2000).

[16] Afanasev, A. M. et al, "Three-crystal diffractometry in Grazing Bragg-Laue geometry", Acta Crystallogr. **A 41**, 227 (1985); Afanasev, A.M., et al, "Asymptotic Bragg diffraction. Single-crystal surface-adjoining-layer structure analysis", Acta Crystallogr., 42, 116 (1986).

[17] Robinson, I. K., "Crystal truncation rods and surface roughness", Phys. Rev. B 33, 3830 (1986).